© 2017. Published by The Company of Biologists Ltd | Journal of Cell Science (2017) 130, 1017 doi:10.1242/jcs.202234

CORRECTION

# Correction: RhoA regulates actin network dynamics during apical surface emergence in multiciliated epithelial cells

**Jakub Sedzinski, Edouard Hannezo, Fan Tu, Maté Biro and John B. Wallingford**

There was an error published in *J. Cell Sci.* **130**, 420-428.

The affiliations were incorrect for the author Maté Biro. The correct author affiliations are as given below.

Jakub Sedzinski[1], Edouard Hannezo[2,3], Fan Tu[1], Maté Biro[4,5] and John B. Wallingford[1,*]

[1]Department of Molecular Biosciences, University of Texas at Austin, Austin, TX 78712, USA.

[2]Cavendish Laboratory, Department of Physics, J.J. Thomson Avenue, University of Cambridge, Cambridge CB3 0HE, UK.

[3]Wellcome Trust/Cancer Research UK Gurdon Institute, University of Cambridge, Tennis Court Road, Cambridge CB2 1QN, UK.

[4]EMBL Australia, Single Molecule Science node, School of Medical Sciences, The University of New South Wales, Sydney, NSW 2052, Australia.

[5]Centenary Institute, Sydney Medical School, The University of Sydney, Sydney, New South Wales 2006, Australia.

*Author for correspondence (Wallingford@austin.utexas.edu)

The authors apologise to the readers for any confusion that this error might have caused.

© 2017. Published by The Company of Biologists Ltd | Journal of Cell Science (2017) 130, 420-428 doi:10.1242/jcs.194704

RESEARCH ARTICLE

# RhoA regulates actin network dynamics during apical surface emergence in multiciliated epithelial cells

**Jakub Sedzinski[1], Edouard Hannezo[2,3], Fan Tu[1], Maté Biro[4,5] and John B. Wallingford[1,*]**


## ABSTRACT

Homeostatic replacement of epithelial cells from basal precursors is a multistep process involving progenitor cell specification, radial intercalation and, finally, apical surface emergence. Recent data demonstrate that actin-based pushing under the control of the formin protein Fmn1 drives apical emergence in nascent multiciliated epithelial cells (MCCs), but little else is known about this actin network or the control of Fmn1. Here, we explore the role of the small GTPase RhoA in MCC apical emergence. Disruption of RhoA function reduced the rate of apical surface expansion and decreased the final size of the apical domain. Analysis of cell shapes suggests that RhoA alters the balance of forces exerted on the MCC apical surface. Finally, quantitative time-lapse imaging and fluorescence recovery after photobleaching studies argue that RhoA works in concert with Fmn1 to control assembly of the specialized apical actin network in MCCs. These data provide new molecular insights into epithelial apical surface assembly and could also shed light on mechanisms of apical lumen formation.


**KEY WORDS: Apical emergence, Actin, Arp2/3, RhoA, Fmn1, Multiciliated cells**

## INTRODUCTION

Epithelia, as dynamic scaffolds and as the first line of defence against toxins and pathogens, are crucial components of all metazoan animals. These cell sheets are characterized both by their barrier function and also by their strong polarization, with a basal surface generally abutting an extracellular matrix and an apical surface facing either a fluid-filled lumen or the exterior of the animal. To maintain homeostatic cell number and organization, epithelial cells undergo turnover – routine addition of new cells and removal of old cells (Macara et al., 2014; Pellettieri and Sanchez Alvarado, 2007).

Epithelial cell turnover poses unique challenges, and simply maintaining a fluid-tight barrier during cell division requires a tight choreography between cells (for example, see Higashi et al., 2016). More complex epithelia face even greater difficulties. For example, the mammalian airway epithelium is maintained through regular addition of new multiciliated cells (MCCs) from a distinct basally positioned population of stem cells, such that nascent cells must first define an apical–basal axis, move apically, insert into the epithelium, and finally assemble an apical cell surface (Fig. 1A) (Rock et al., 2009, 2010; Watson et al., 2015). Although the establishment of apicobasal polarity and the assembly of apical cell surfaces during lumen formation have been extensively studied (Datta et al., 2011; Rodriguez-Boulan and Macara, 2014), the mechanisms by which individual nascent cells insert into an epithelium and by which a new apical cell surface emerges remain poorly characterized.

Recently, the nascent MCCs in developing *Xenopus* embryos have emerged as a model for studies of mucociliary epithelia (Werner and Mitchell, 2011). These epithelial cells, which display dozens or hundreds of synchronously beating cilia that generate fluid flow across epithelium, are born from a population of basal progenitor cells (Drysdale and Elinson, 1992). They subsequently intercalate radially into the superficial epithelium, where they integrate with the pre-existing epithelial cells and expand their apical surface (Fig. 1A) (Stubbs et al., 2006). An outline of the molecular framework for the control of radial intercalation of MCCs is now emerging, revealing key roles for dystroglycan, Rab11, the Par complex, Slit2 and the Rfx2 transcription factor (Chung et al., 2014; Kim et al., 2012; Sirour et al., 2011; Werner et al., 2014). In addition, we have recently explored the mechanical basis specifically of apical surface emergence in nascent MCCs, finding that the forces that drive apical emergence are cell-autonomous and dependent on the assembly of an apical actin network generating effective two-dimensional (2D) pushing forces (Sedzinski et al., 2016).

MCCs are known to develop complex apical actin structures that are not shared with the neighboring mucus-secreting cells into which they emerge, an attribute observed not only in *Xenopus* (Park et al., 2006; Sedzinski et al., 2016; Turk et al., 2015; Werner et al., 2011) but also in MCCs of the mouse airway and avian oviduct (Chailley et al., 1989; Pan et al., 2007). This actin network is crucial not only for apical emergence in nascent cells (Sedzinski et al., 2016) but also for basal body docking (Park et al., 2008) and basal body planar polarization (Turk et al., 2015; Werner et al., 2011). The molecular mechanisms controlling assembly of this multi-functional actin network remain poorly defined.

For example, the small GTPase RhoA is required for basal body docking and planar polarization (Pan et al., 2007; Park et al., 2006), but its role in MCC apical emergence is unknown. Moreover, the known RhoA effector Formin 1 (Fmn1) is required for apical emergence (Sedzinski et al., 2016), but little else is known about Fmn1 regulation or its mode of action. Here, we combine transgenic reporters, *in vivo* time-lapse imaging and fluorescence recovery after photobleaching (FRAP) to demonstrate that RhoA activity is required in nascent MCCs for normal apical emergence, acting together with Fmn1 to control the dynamics of the MCC apical actin network. These results shed new light on the process of apical

[1]Department of Molecular Biosciences, University of Texas at Austin, Austin, TX 78712, USA. [2]Cavendish Laboratory, Department of Physics, J.J. Thomson Avenue, University of Cambridge, Cambridge CB3 0HE, UK. [3]Wellcome Trust/Cancer Research UK Gurdon Institute, University of Cambridge, Tennis Court Road, Cambridge CB2 1QN, UK. [4]Centenary Institute of Cancer Medicine and Cell Biology, Locked Bag 6, Newtown, New South Wales 2042, Australia. [5]Sydney Medical School, The University of Sydney, Sydney, New South Wales 2006, Australia.

*Author for correspondence (Wallingford@austin.utexas.edu)

J.B.W., 0000-0002-6280-8625

**Received 12 July 2016; Accepted 10 November 2016**

Journal of Cell Science (2017) 130, 420-428 doi:10.1242/jcs.194704

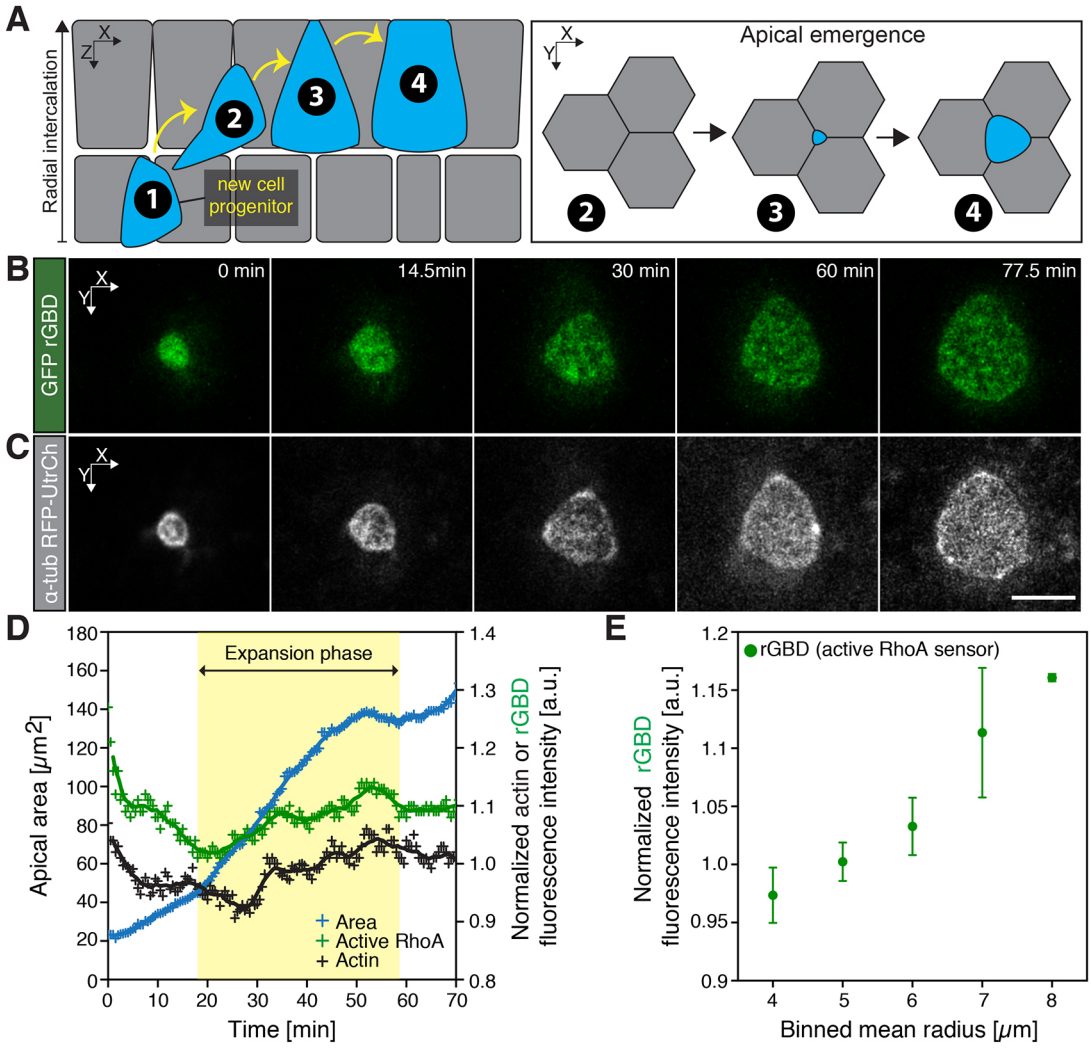


**Fig. 1. Active RhoA localizes to the apical domain of emerging MCCs.** (A) Schematic of MCC morphogenesis. Upon specification of an MCC progenitor (1), a nascent MCC radially intercalates (2, 3) and docks at the tricellular junction to finally integrate with the pre-existing epithelium by expanding its apical surface (3, 4, apical emergence). (B) Image sequence of an active RhoA biosensor (rGBD, green) throughout apical emergence of a single unmanipulated cell. (C) Corresponding image of an apically emerging MCC (visualized using an actin marker, utrophin, GFP–UtrCH, gray, driven by an MCC-specific α-tubulin promoter). (D) Representative plot of medial actin and active RhoA dynamics during apical emergence. (E) Values of the intensity of active RhoA for consecutive categories of apical domain sizes, categorized by the binned mean radius in controls. Data represent mean and s.e.m., $n$=4 cells from four embryos. Actin and rGDB intensities were normalized by dividing the mean intensities of medial actin and/or rGBD by the mean intensities of actin and/or rGBD within the cortical region. Scale bars: 10 µm.

emergence specifically and are also of more general interest because of the broad roles for formin proteins in apical surface remodeling during lumen formation (Grikscheit and Grosse, 2016).

## RESULTS

### RhoA controls the dynamics of MCC apical emergence

Formin proteins contribute to various cellular actin-based cytoskeletal structures through their ability to polymerize linear actin filaments and are commonly recognized as key effectors of Rho GTPases (Goode and Eck, 2007; Hall, 2012). Given the requirement for Fmn1 in apical emergence (Sedzinski et al., 2016), we probed the role of RhoA in this process. We first measured the dynamics of RhoA activity using the active RhoA biosensor (rGBD), which has been shown previously to be effective in *Xenopus* (for examples, see Benink and Bement, 2005; Breznau et al., 2015; Reyes et al., 2014). We expressed GFP–rGBD in the mucociliary epithelium and found that throughout the expansion phase of the MCC apical surface, the fluorescence intensity of normalized active RhoA increased (Fig. 1B–E), a pattern that is highly reminiscent of that observed for apical actin, a key driver of apical emergence (Fig. 1C,D).

To further explore the role of RhoA in MCC apical emergence, we expressed dominant negative (DN-) and constitutively active RhoA (CA-RhoA), specifically in *Xenopus* MCCs using the α-tubulin (*Tuba4b*) promoter (Stubbs et al., 2006). This approach allowed us to assess the effect of two opposite regimes, either higher or lower RhoA activity, in a cell-autonomous manner in emerging MCCs. We observed that expression of DN-RhoA slowed the rate of apical surface area expansion and decreased the final size of the MCC apical domain, whereas expression of CA-RhoA had no significant effect (Fig. 2; Fig. S1). In addition, DN-RhoA-expressing cells also exhibited non-periodic iterative pulses of expansion and constriction of the apical surface (Fig. 2C,D; Table S1, Movie 1). These pulses were similar to those observed after disruption of Fmn1 function; importantly, however, expression of DN-RhoA rarely elicited the complete collapse of the apical cell

Journal of Cell Science (2017) 130, 420-428 doi:10.1242/jcs.194704

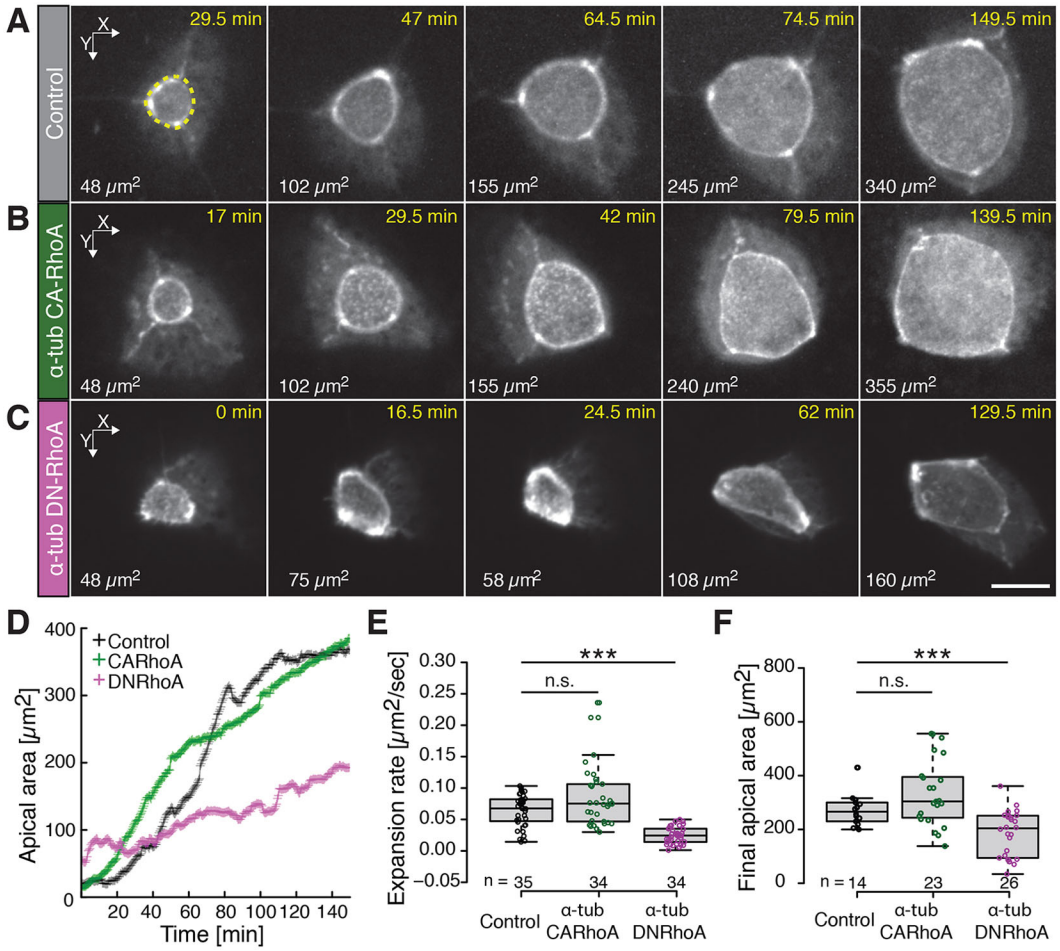


**Fig. 2. RhoA controls the dynamics of MCC apical emergence.** (A) Image sequence of an apically emerging MCC (visualized using an actin marker, utrophin, GFP–UtrCH, gray, driven by an MCC-specific α-tubulin promoter) in controls, (B) upon expression of a constitutively active RhoA construct (CA-RhoA) and (C) upon expression of dominant negative RhoA (DN-RhoA). CA-RhoA and DN-RhoA were expressed in MCCs under an MCC-specific α-tubulin promoter, see Fig. S1. Quantification of MCC apical surface area (e.g. dotted yellow line in A) is indicated in $\mu m_2$ in the bottom left corner of each panel. Note that for a given apical domain surface, an apical domain of an MCC expressing DN-RhoA has a more polygonal shape compared to that of controls and to an MCC expressing CA-RhoA. (Note that an image in Fig. 2A is replicated in Fig. 4B; see Fig. 4 legend for details). The time after the start of imaging is indicated. (D) Dynamics of the apical domain area of the MCCs shown in A–C; controls, black; MCC expressing CA-RhoA, green; MCC expressing DN-RhoA, pink. (E) Expansion rate of an MCC apical domain in controls (black) and upon expression of CA-RhoA (green) or of DN-RhoA (magenta). The expansion rate was determined by measuring the slope of the linear fit of the surface area data between 50 $\mu m^2$ and 150 $\mu m^2$. (F) The final apical domain areas of MCCs under the conditions described in E. Boxes extend from the 25th to 75th percentiles, with a line at the median. Whiskers represent the minimum and maximum values. ***$P$<0.001; n.s., not significant (Mann–Whitney U test). $n$>5 embryos; $n$ values on the graph represent the number of cells analyzed. Scale bar: 10 μm.

surface that is associated with formin loss in these cells (Table S1) (Sedzinski et al., 2016). This difference might result from the efficacy of the reagents [DN-RhoA versus a morpholino against Fmn1 (Fmn1-MO)] in decreasing the actin-based pushing forces, or it could relate to the specific functions of the two proteins in controlling force balance at the MCC apical surface, as we discuss below.

Formins are known to act as RhoA effectors in diverse settings, so we next examined the localization and dynamics of Fmn1 after DN-RhoA expression. We found that in controls fluorescently tagged Fmn1 was evenly distributed throughout the apical domain (Fig. S2A,E,I), whereas cells expressing DN-RhoA accumulated Fmn1 predominantly within the central portion of the apical cell surface (Fig. S2C,G,J). Similarly, expression of DN-RhoA resulted in a higher concentration of actin within the central region of the apical domain (Fig. S2C,G,J) compared to the uniform actin signal in controls (Fig. S2B,F,I). We then measured the dynamics of Fmn1 and actin, and observed that expression of DN-RhoA impaired both stereotypical patterns (Fig. S2K,L). Taken together, these data suggest that RhoA works upstream of Fmn1 and is required in a cell-autonomous manner for normal apical emergence in MCCs.

## RhoA controls force balance in the apical surface during MCC emergence

We next sought to understand how manipulation of RhoA in MCCs impacted upon the mechanical forces that drive apical emergence. MCC apical emergence in *Xenopus* is the product of the force balance exerted on an apical cell membrane by cell-autonomous and cell-non-autonomous forces (Fig. 3A). Emergence is facilitated by (i) actin-based pushing forces (2D pressure) generated by actin network assembly within the medial portion of the MCC apical domain (Fig. 3A, orange arrows, δP) and (ii) pulling forces, generated by actomyosin cortical tension of the perpendicular junctions along neighboring cells (Fig. 3A, blue arrows, Λ). Conversely, emergence is resisted by (i) actomyosin-based cortical tension within the MCC that acts to shrink the apical domain

Journal of Cell Science (2017) 130, 420-428 doi:10.1242/jcs.194704

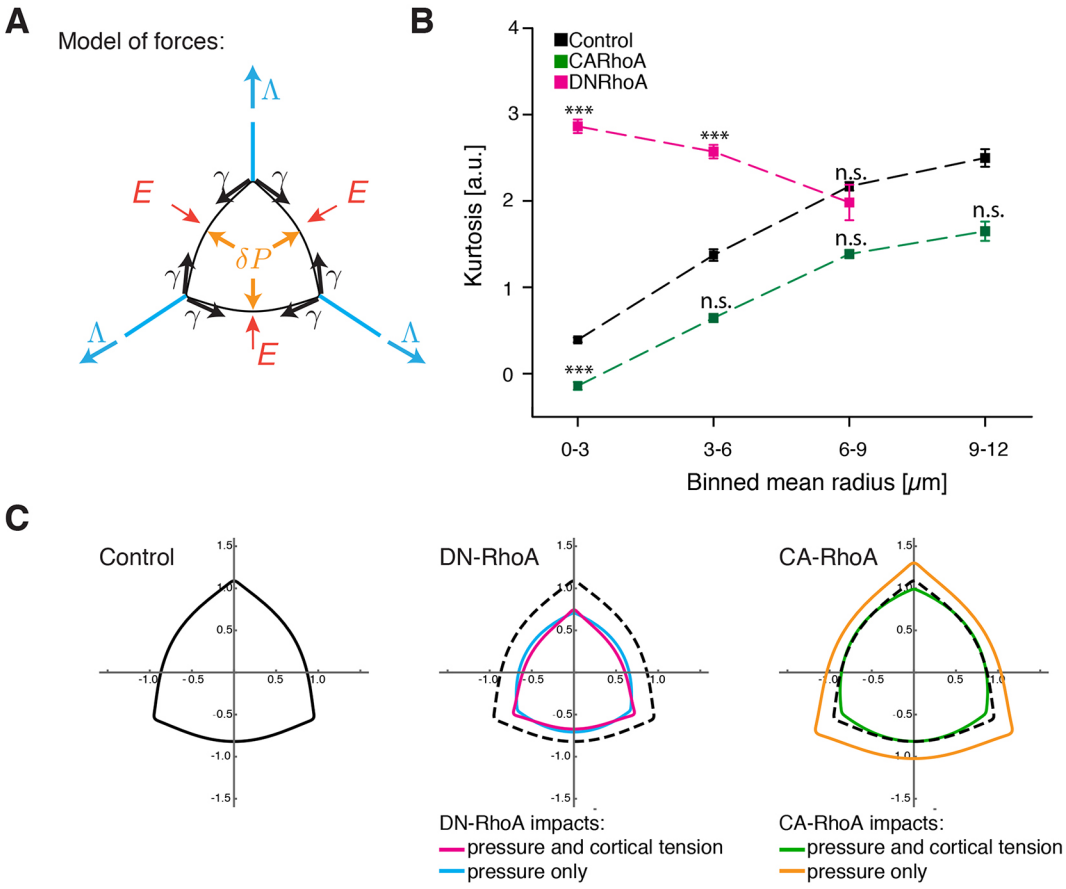


**Fig. 3. RhoA controls force balance in the apical surface during MCC emergence.** (A) Schematic of forces acting on an MCC apical domain. Effective 2D pressure, δP (orange arrows), and junctional pulling forces, Λ (blue arrows), acting against cortical tension, γ (black arrows), and elasticity from the surrounding cells, *E* (red arrows). (B) Kurtosis values for the consecutive categories of apical domain sizes, categorized by binned mean radius, in controls and cells expressing DN-RhoA or CA-RhoA. Data represent mean±s.e.m. ***$P$<0.0005; n.s., not significant (two-tailed unpaired Student's *t*-test). $n$=10 cells, $n$>5 embryos. (C) Simulations of apical domain shapes upon expression of DN-RhoA or CA-RhoA. The simulations assumed that only pressure or both pressure and cortical tension were impacted upon expression of the different RhoA constructs. The final shapes of the apical domains are each represented by a different color.

(Fig. 3A, black arrows, γ) and (ii) resistance of the neighboring cells (Fig. 3A, red arrows, *E*) (Sedzinski et al., 2016).

The respective contributions of these forces can be assessed by analyzing the shape and dynamic behavior of the apical cell perimeter. When considering cell autonomous forces within the MCCs, apical surface perimeters are rounded when pushing forces dominate but are polygonal when pulling forces are in excess. Moreover, apical perimeters collapse when MCC cortical tension (γ) exceeds the pushing forces (δP). For example, such collapses are consistently observed after disruption of Fmn1 by knockdown, expression of a dominant-negative construct or pharmacological inhibition (Sedzinski et al., 2016). Generically, the curvature of an MCC cell edge is determined by the ratio of the pressure difference between the MCC and the neighboring cell sharing this edge, and by the MCC cortical tension, a relationship known as the Laplace law. To interrogate the balance of forces in MCCs after manipulation of RhoA function, we quantified apical surface shapes by segmenting the apical perimeter and calculating the kurtosis of its curvature; kurtosis here is thus an angularity parameter, which equals zero if the domain is perfectly round and increases for more polygonal shapes (Movie 1; see Materials and Methods).

Normally, the apical surfaces of MCCs are rounded (low kurtosis) during early emergence, indicating that pushing forces dominate at these stages (Figs 2A and 3B, black) (Sedzinski et al., 2016). By contrast, apical domain shapes of MCCs expressing DN-RhoA were more polygonal, with elongated cell–cell boundaries meeting at sharp junctional angles (Figs 2C, 3B, pink). This effect was particularly pronounced at during early stages of emergence (i.e. small apical domains). This polygonal cell shape suggests that the predominant effect of DN-RhoA in MCCs is a reduction of the pushing force (δP), leading to defective apical emergence.

To further test the impact of expression of DN-RhoA, we performed shape simulations testing the possibilities that RhoA acts only on apical actin assembly (pressure) or both on apical actin assembly and MCC cortical tension. We assume that a decrease in pressure causes a decrease in MCC area and that a decrease in MCC cortical tension has the opposite effect. Because we observed a significantly lower final area for MCCs that expressed DN-RhoA, we conclude that the reduction of pressure must outweigh the decrease of cortical tension. However, decreasing both pressure and MCC tension cooperate in increasing the angularity of the MCC, and our simulations suggest that DN-RhoA-expressing cells also slightly downregulate MCC cortical tension to account for their angularity increase (Fig. 3C).

Interestingly, we also observed that expression of CA-RhoA *in vivo* did not significantly change the kurtosis parameter compared to that of controls of similar areas (Figs 2B, 3B, green), with the exception of small apical areas, for which CA-RhoA-expressing

Journal of Cell Science (2017) 130, 420-428 doi:10.1242/jcs.194704

cells were more round. Moreover, CA-RhoA-expressing MCCs did not display a significantly larger final apical area. A plausible explanation for this phenomenon would be that RhoA is already fully activated in control cells. Another hypothesis would be that CA-RhoA slightly increases both the MCC apical pushing force (δP) and also the MCC cortical tension (γ), resulting in a slightly rounded cell shape, with the influence of each on rate and final area of apical emergence cancelling each other, a scenario predicted by the shape simulations (Fig. 3C). Taken together, these data suggest that RhoA regulates both 2D pressure and cortical tension in MCCs, and that the dynamics of apical emergence are the net product of these forces.

### RhoA controls the rate of MCC apical actin network assembly

MCC emergence is characterized by a strong positive correlation between apical area and apical actin concentration, suggesting that the apical actin network assembly drives emergence (Sedzinski et al., 2016). We therefore assessed the effect of RhoA manipulation on actin network assembly in MCCs by measuring apical actin concentration over time (Fig. 4A–C; Movie 1) (see Materials and Methods). In controls, we observed a consistent increase in apical actin intensity across the period of emergence (Fig. 4C, black), as reported previously. Likewise, we observed no change in actin assembly after expression of CA-RhoA (Fig. 4C, green). In striking contrast, expression of DN-RhoA significant abrogated apical actin assembly (Fig. 4C, pink). As a result, the clear positive linear correlation between apical surface area and normalized actin intensity that we observed in normal cells was dramatically reduced in in MCCs that expressed DN-RhoA (Fig. 4D). These data suggest that RhoA is an essential positive regulator of apical actin assembly during MCC emergence, and that in the absence of RhoA function, failure of actin assembly (Fig. 4) results in a reduced pressure δP (Fig. 3), which in turn disturbs apical emergence (Fig. 2).

### RhoA and Fmn1 control actin turnover rate in the MCC apical actin network

The apical actin network of MCCs is highly specialized (Park et al., 2006; Sedzinski et al., 2016; Turk et al., 2015; Werner et al., 2011). However, unlike well-studied actin networks such as lamellipodia, we know almost nothing about the molecular control of MCC apical actin assembly. We therefore sought to characterize the dynamics of this actin population, which can be done by quantifying the turnover of apical actin in MCCs using fluorescence recovery after photobleaching (FRAP) of YFP–actin (Fritzsche et al., 2013; Grikscheit et al., 2015; Phng et al., 2015; Sahasrabudhe et al., 2016). We photobleached a small region of interest within a medial portion of MCC apical domains and monitored subsequent recovery of YFP–actin fluorescence (Fig. 5A,B). Compared to the well-characterized actin networks of lamellipodia or of the cell cortex (Lai et al., 2008; Watanabe, 2010), fluorescence recovery of the MCC apical actin network was much slower, suggesting that the MCC apical actin network is very stable.

Strikingly, cells that expressed DN-RhoA displayed an initial slope of fluorescence actin recovery that was steeper than that of controls, and accordingly, the half-time of fluorescence recovery was shorter (Fig. 5C,D). These data argue that in the specialized apical actin network of MCCs, inhibition of RhoA results in increased actin turnover. Formins are well known effectors of RhoA activity (Goode and Eck, 2007; Hall, 2012), so in light of the requirement for both RhoA and Fmn1 in apical emergence, we examined the effect of Fmn1 knockdown on apical actin dynamics by FRAP. Fmn1 knockdown also significantly accelerated the half-time of recovery of YFP–actin after photobleaching (Fig. 5C,D). Interestingly, we observed no difference between the recovery curves of CA-RhoA and of controls (Fig. 5C,D). In all conditions, the immobile fraction was small and did not differ significantly between conditions (Fig. 5D).

Recently, several studies have suggested that actin turnover rates are impacted by a finite balance of actin filament subpopulations, with distinct turnover kinetics regulated by ARP2 and ARP3 (Arp2/3) and formins. In this scheme, inhibition of formins or Arp2/3 shifts the turnover rate towards the Arp2/3- or formin-based kinetics, respectively (Burke et al., 2014; Fritzsche et al., 2013; Lomakin et al., 2015; Rotty et al., 2015; Suarez et al., 2015). To determine if such a balance was also at work in MCCs *in vivo*, we performed FRAP on apical actin after treatment with a specific Arp2/3 inhibitor, CK666. In contrast to the effects of Fmn1 or RhoA disruption, we observed that inhibition of Arp2/3 decreased the half time of actin turnover and also reduced the mobile fraction (Fig. 5C–E). This result could be explained by the fact that formin-nucleated filaments are, on average, ten times longer than Arp2/3-nucleated filaments, thus their turnover is slower (Fritzsche et al., 2016). Consequently, inhibition of Arp2/3 shifts the actin kinetics toward a slower turnover rate, whereas knockdown of Fmn1 facilitates nucleation of shorter actin filaments turning over more quickly. Indeed, loss of Fmn2 has been associated with the presence of shorter actin filaments, which turnover more quickly (Yang et al., 2007).

## DISCUSSION

Here, we have examined the function of RhoA and the dynamics of the apical actin network during apical emergence in nascent MCCs. These data build on our previous work that has shown that the force balance between a pushing apical actin network and actomyosin cortex contractility determines the dynamics of MCC emergence (Sedzinski et al., 2016). Our data suggest that RhoA acts in concert with Fmn1 and that Fmn1 acts in balance with Arp2/3 to control assembly of the MCC apical actin network.

We found that depletion of Fmn1 specifically in MCCs leads to apical domain collapse as a consequence of high cortical tension and low actin-based pushing forces (Fig. 6A, blue) (Sedzinski et al., 2016), so it is relevant that RhoA regulates both contractile processes through activation of myosin motors through Rho kinases and also actin polymerization through formins (Goode and Eck, 2007; Hall, 2012). Here, our imaging of the dynamics of apical emergence (Fig. 2), analysis of cell shapes (Fig. 3) and dynamics of apical actin (Figs 4 and 5) indicate that expression of DN-RhoA decreases formin-mediated actin network assembly, which leads to a slower expansion rate and polygonal shape of the apical domain (Fig. 6B, pink). The fluctuations of apical area without total collapse that are elicited by DN-RhoA is a milder phenotype compared to the effect of Fmn1 disruption, which is probably due to a simultaneous effect of RhoA disruption on both cortical contractility – the driving force of collapse – and actin-based pushing (Fig. 6B, pink). Interestingly, expression of CA-RhoA had no general impact on the process of apical emergence; perhaps suggesting that in control cells RhoA is maintained at a fully activated state (Fig. 6A, green). In the future, it will be important to further decipher Fmn1 regulation, particularly to identify molecular switches that direct RhoA toward activation of actin polymerization in the apical surface and activation of myosin motors at the cortex.

The results of our analysis of actin turnover are also of interest because we find that Fmn1 loss leads to acceleration of actin

Journal of Cell Science (2017) 130, 420-428 doi:10.1242/jcs.194704

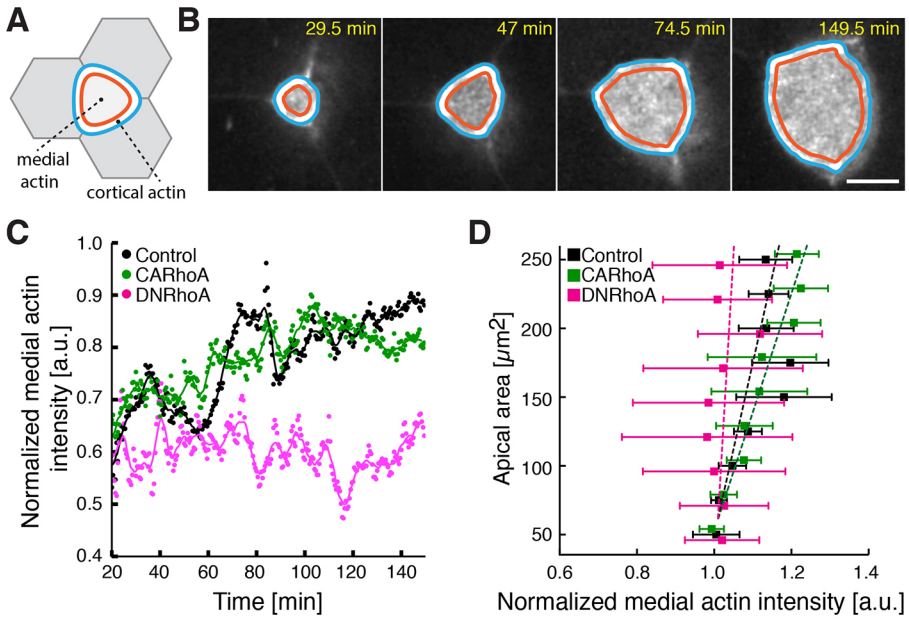


**Fig. 4. RhoA controls the rate of MCC apical actin network assembly.** (A) Schematic of the medial and cortical regions within an apical domain of an MCC. (B) A representative image sequence of an automatically segmented cortical and medial region within an apically expanding MCC (visualized using α-tubulin-promoter-driven GFP–UtrCH, gray). Note that the image here is replicated from Fig. 2A as an example. The time after the start of imaging is indicated. Scale bar: 10 µm. (C) Apical actin concentration (ratio of mean medial to mean cortical actin) dynamics in a control cell (black), an MCC expressing CA-RhoA (green) and an MCC expressing DN-RhoA (magenta). Circles, data points; lines, data smoothed with a moving average of 5. (D) Apical actin concentration as a function of apical area in control cells, in MCCs expressing CA-RhoA and MCCs expressing DN-RhoA; $n$>10 cells from $n$>5 embryos. Data represent mean and s.e.m. The slope for MCCs expressing DN-RhoA (pink dotted line) is significantly higher than that for control ($P$<0.05, Z-test for correlation coefficients), whereas the slope for MCCs expressing CA-RhoA is not significantly different from that of control.

turnover, and disruption of another formin, Fmnl2, has been shown to have a similar effect on cortical actin in epithelial cells (Grikscheit et al., 2015). However, our results contrast with recent data that show that inhibition of formins increases the half time of actin turnover in other cell types, including M2 melanoma cells, neurons, vascular cells and fibroblasts (Fritzsche et al., 2013; Ganguly et al.,

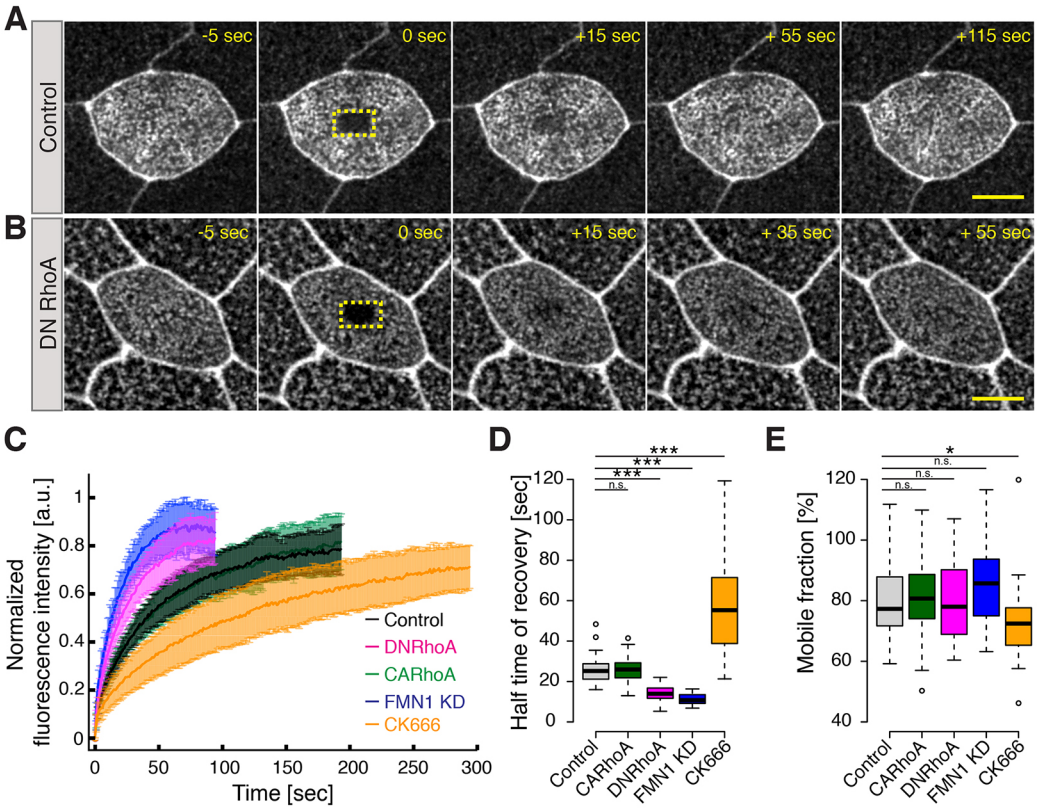


**Fig. 5. RhoA, FMN1 and Arp2/3 control the rate of turnover of actin in the MCC apical actin network.** (A) Image sequence of an MCC apical domain in a control cell and (B) in a cell expressing DN-RhoA, visualized using monomeric YFP–actin upon photobleaching of a region of interest (dotted yellow line) within the medial portion of the apical domain. 0 s indicates the time of photobleaching. (C) Normalized actin recovery after photobleaching (FRAP) of monomeric actin within the medial portion of an apical domain of MCCs: in control cells (black), cells expressing CA-RhoA (green), cells expressing DN-RhoA (red), FMN1-knockdown cells (FMN1 KD; blue) and upon Arp2/3 inhibition with CK666 (orange). Data are mean±s.d. (D) Fluorescence half-time recovery after photobleaching of medial actin in controls (black), MCCs expressing CA-RhoA (green), MCCs expressing DN-RhoA (magenta), FMN1-knockdown cells (blue) and upon Arp2/3 inhibition with CK666 (orange). (E) The mobile fraction measured upon FRAP analysis of medial actin under the conditions described in D. Boxes extend from the 25th to 75th percentiles, with a line at the median. Whiskers indicate minimum and maximum values. *$P$<0.05; ***$P$<0.001; ns, not significant (Mann–Whitney U test). $n$>5 embryos. Scale bars: 10 µm.

Journal of Cell Science (2017) 130, 420-428 doi:10.1242/jcs.194704

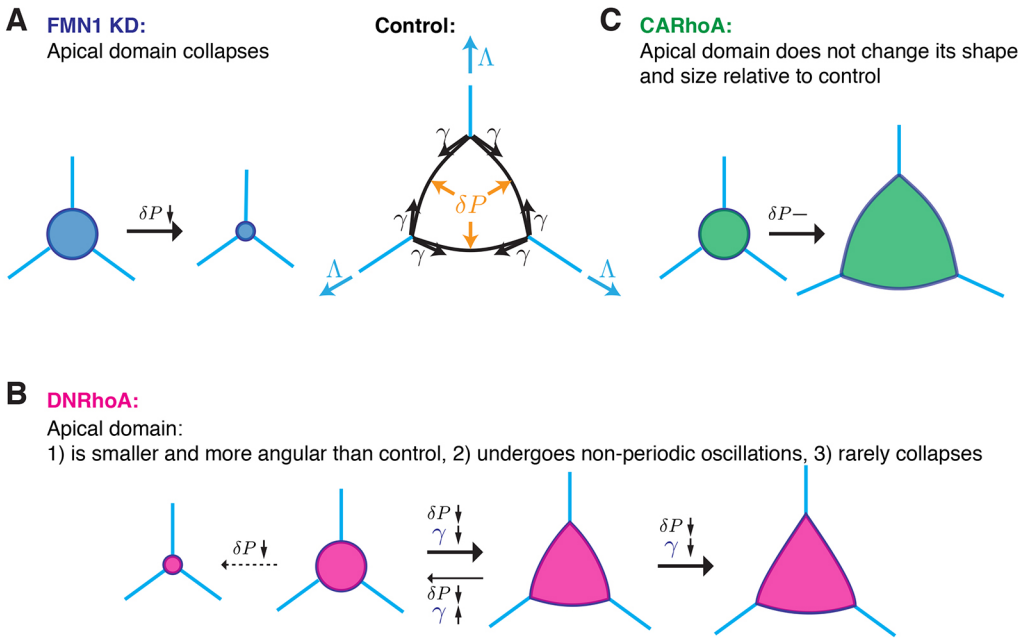


**Fig. 6. Different modes of apical emergence depend on RhoA activity.** (A) Upon knockdown of Fmn1 (FMN1 KD), the apical domain collapses as a consequence of low pushing forces and high cortical tension. (B) Expression of DN-RhoA decreases both pushing forces and cortical tension. Depending on the net contribution of these forces, the apical domain (i) expands in an angular manner to an overall smaller size, (ii) undergoes non-periodic oscillations, (iii) collapses. (C) Expression of CA-RhoA does not change the dynamics of apical emergence.

2015; Phng et al., 2015; Sahasrabudhe et al., 2016). Clearly, however, the functions of formin proteins differ between cell types and actin populations, because loss of formins decreased the mobile actin fractions in fibroblasts and neurons (Ganguly et al., 2015; Sahasrabudhe et al., 2016) yet left the mobile fraction unchanged in vascular cells (Phng et al., 2015), similar to the case here for MCCs. Moreover, in systems in which an actin network forms *de novo*, such as in the cortex of retracting blebs, actin turnover is almost tenfold higher compared with that in the mature cortex, suggesting that the molecular mechanisms regulating actin turnover in new cortices are different compared to those in mature networks (Bovellan et al., 2014). It is important to note, therefore, that the FRAP analyses reported here were performed on mature apical MCC surfaces. The dynamics of apical actin during the active expansion of the apical MCC surface could be different and should be explored. Nevertheless, the findings here also suggest that Fmn1 works in counterbalance with Arp2/3 to control the MCC apical actin network, as has been observed in other cell types (Burke et al., 2014; Rotty et al., 2015; Suarez et al., 2015). Thus, our data argue that the MCC apical actin network, like other well-defined actin structures, is quite complex. Additional studies will be required to fully understand how this network is regulated to execute its diverse functions, not only during MCC apical emergence but also during ciliogenesis and basal body polarization and positioning (Park et al., 2006; Sedzinski et al., 2016; Turk et al., 2015; Werner et al., 2011).

Finally, our data here highlight the similarities between distinct modes of apical surface remodeling. Studies in diverse vertebrate cell types *in vitro* and *in vivo* demonstrate a key role for formins in coordinating apical surface formation among groups of cells during epithelial lumen formation (Grikscheit et al., 2015; Madrid et al., 2010; Phng et al., 2015; Taniguchi et al., 2015). Likewise, our data here and in previous work (Sedzinski et al., 2016) demonstrate a similar requirement for formins in the emergence of an individual apical epithelial surface in MCCs. Interestingly, the coordinated assembly of multiple apical surfaces during lumen formation also requires Rab11, the Par complex and Slit–Robo signaling (Bryant et al., 2010; Medioni et al., 2008; Santiago-Martinez et al., 2008), and the same is true of radial intercalation and apical emergence in individual MCCs (Chung et al., 2014; Kim et al., 2012; Werner et al., 2014). Further exploration of these issues will provide new insights into the mechanisms of organogenesis and epithelial homeostasis.

## MATERIALS AND METHODS

### *Xenopus* embryo manipulations

Experiments were performed following the animal ethics guidelines of the University of Texas at Austin, protocol number AUP-2015-00160. *Xenopus laevis* adult females were induced to ovulate through injection of human chorionic gonadotropin. The following day, eggs were squeezed, fertilized *in vitro* and dejellied in 3% cysteine (pH 7.9). Fertilized embryos were washed and subsequently reared in a 0.3× Marc's Modified Ringer's (MMR) solution. For microinjections, embryos were placed into a solution of 2% Ficoll in 0.3× MMR and injected using a glass capillary-pulled needle, forceps and an Oxford universal micromanipulator.

### Cloning, plasmids, morpholinos and drug treatment

For α-tubulin-driven expression of DN-RhoA or CA-RhoA, the open reading frame (ORF) of human DN-RhoA or CA-RhoA was amplified by performing PCR from plasmids obtained from addgene.org (#15901 and #15900, respectively), enzymatically subcloned into a α-tubulin-driven expression plasmid containing a C-terminal RFP expression tag, and injected into two ventral blastomeres at the four-cell stage at 30 pg per blastomere. We observed no differences in phenotype upon fluorescently tagging the CA-RhoA sequence at the N-terminal end. Apical actin was visualized using α-tubulin-driven GFP–utrophin (GFP–UtrCH) injected at 25 pg per blastomere. Morpholinos against Fmn1 were used as described previously (Sedzinski et al., 2016). Arp 2/3-mediated actin polymerization was inhibited by incubating for 30 min with 50 µM CK666 (Sigma).

### Live imaging of apical expansion

Embryos at stages ∼18–20 were mounted in 0.8% (w/v) low-melting-point agarose (LMPA), covered in 0.3× MMR and imaged at 23°C with a Zeiss LSM700 confocal microscope using C-Apochromat 40× 1.2 NA water immersion objective.

### Fluorescence recovery after photobleaching

FRAP experiments were performed on a laser scanning confocal microscope Zeiss LSM 700 using a Plan-Apochromat 63×1.4 NA Oil DIC M27 objective lens (Zeiss). Stage 23–24 YFP–β-actin-expressing embryos (injection of 50 pg of mRNA per ventral blastomer) were mounted in 0.8% (w/v) LMPA and immersed in 0.3× MMR. A region of interest (ROI) with the dimensions

4.5×3 µm of a YFP–β-actin-expressing MCC was bleached using: 100% power of a 488-nm laser and a 3.15-µsec pixel dwell time within the ROI. Fluorescence recovery was monitored for up to 200 frames (1 s/frame), bleach corrected and normalized with a custom written code in Python (modified from http://imagej.net/Analyze_FRAP_movies_with_a_Jython_script). We assume that the time evolution of the actin density ρ is given by the simple first order kinetics equation:

$$\frac{d\rho}{dt} = k_p - k_d\rho = -\frac{1}{\tau}(\rho - \rho_0),$$

where we defined $k_p$ as the polymerization rate, $k_d$ as the depolymerization rate, $\tau = 1/k_d$ as the turnover rate and $\rho_0 = k_p/k_d$ as the steady-state actin density.

This predicts a single exponential with characteristic time τ for the recovery curves, which we have verified here experimentally. Moreover, one can see from the equation above that the turnover time is inversely proportional to the depolymerization rate. Therefore, a lower turnover time in Fmn1-MO and α-tubulin-driven DN-RhoA embryos indicates a higher depolymerization rate. In turn, assuming a steady polymerization rate, this leads to a lower actin density $\rho_0$.

## Image processing and automated image analysis

Images were processed and automatically analyzed using a custom code in MATLAB (KoreTechs), as previously described (Biro et al., 2013).

### Cell contour detection and classification of cellular regions

Segmentation of cells was based on a combination of image filtering, ellipse fitting and adaptive thresholding. Throughout images and movies, as we were looking at a 2D representation of a 3D cell, of which only the apical surface was exposed, this apical surface in reality constitutes a cortical surface. However, within the focused apical plane, the cortex was defined as a region of fixed depth underlying the segmented cell contour. The medial region was taken as the difference between the segmented cell area and the cortical region. The definition of the cell contour, cortical and cytoplasmic regions allowed for the extraction of region-specific morphological parameters and intensity values. The effective apical actin concentration and amount of active RhoA were defined as a ratio of the mean actin:rGBD intensity in the medial region and as the mean intensity of actin:rGBD within cortical region.

## Measuring angularity of the apical domain by kurtosis

In order to have a quantitative measurement of the angularity of MCC apical perimeter over time, we segmented the outline of the cell apical perimeter and calculated it in polar coordinates r(\Θ,t), using a 1 degree binning. After smoothing the function r(\Θ,t) with a 5° binning over \Θ, we calculated the local curvature C(\Θ,t), and we then computed the kurtosis k(t) of the distribution C(\Θ,t) – i.e. the normalized fourth moment minus 3 (the reason for subtracting 3 is that it is the kurtosis of a normal distribution, which is expected to arise purely from segmentation noise and errors). We then binned the data for given apical radii and averaged each bin across all cells analyzed. The rationale for using radius instead of time as the *x*-axis is to correct for the difference in timing of apical emergence between different cells. To statistically compare kurtosis at each radius between mutant and control, we compared each distribution of average kurtosis among different cells by performing Welch's *t*-test. Our reasoning for using kurtosis as an indicator of angularity is that it measures how heavy the tails are of a distribution. Very angular cells will have mostly low curvature at the edges but very high curvatures at their vertices, resulting in a heavy-tailed distribution, and thus high kurtosis. In contrast, round cells will have a kurtosis close to 0. This makes rescaled kurtosis a more intuitive measurement than the variance of the distribution, for instance.

## Statistical analyses

Statistical analyses were performed using MATLAB software. Unless otherwise specified, Mann–Whitney U-test was used to compare statistical significance. The experiments were not randomized, and no statistical method was used to predetermine sample size. Reproducibility of all results was confirmed by performing independent experiments. All experiments were repeated a minimum of three times. To statistically compare the area versus actin concentration curves in different experiments, we used linear least square regression to obtain estimates for the slope and standard error of the slope in each condition, and tested for statistical differences between the slope of the control versus a given mutant condition.

### Acknowledgements

We thank the Wallingford laboratory members for experimental suggestions and critical reading of the manuscript.

### Competing interests

The authors declare no competing or financial interests.

### Author contributions

J.S., E.H. and J.B.W. designed the research and wrote the paper; J.S. performed the experiments; M.B. developed the image analysis tools; J.S., E.H. analyzed the data; F.T. contributed to experimental procedures.

### Funding

This work was funded by a European Molecular Biology Organization (EMBO) Long Term Fellowship to J.S.; a Research Fellowship from Trinity College, University of Cambridge; a Wellcome Trust fellowship (110326/Z/15/Z) and Fondation Bettencourt Schueller Young Researcher Prize to E.H; a Cancer Institute NSW Early Career Researcher fellowship (13/ECF/1-25) and a Cancer Australia and Cure Cancer Australia Foundation project grant (1070498) to M.B.; and grants from the National Heart, Lung, and Blood Institute (HL117164) and National Institute of General Medical Sciences (GM074104) to J.B.W. This work was initiated at the New Quantitative Approaches to Morphogenesis Workshop at University of California, Santa Barbara, which is funded in part by the National Science Foundation (PHY11-25915) and the National Institute of General Medical Sciences (GM067110-05). Deposited in PMC for release after 12 months.

### Supplementary information

Supplementary information available online at
http://jcs.biologists.org/lookup/doi/10.1242/jcs.194704.supplemental

### References

**Benink, H. A. and Bement, W. M.** (2005). Concentric zones of active RhoA and Cdc42 around single cell wounds. *J. Cell Biol.* **168**, 429-439.

**Biro, M., Romeo, Y., Kroschwald, S., Bovellan, M., Boden, A., Tcherkezian, J., Roux, P. P., Charras, G. and Paluch, E. K.** (2013). Cell cortex composition and homeostasis resolved by integrating proteomics and quantitative imaging. *Cytoskeleton (Hoboken)* **70**, 741-754.

**Bovellan, M., Romeo, Y., Biro, M., Boden, A., Chugh, P., Yonis, A., Vaghela, M., Fritzsche, M., Moulding, D., Thorogate, R. et al.** (2014). Cellular control of cortical actin nucleation. *Curr. Biol.* **24**, 1628-1635.

**Breznau, E. B., Semack, A. C., Higashi, T. and Miller, A. L.** (2015). MgcRacGAP restricts active RhoA at the cytokinetic furrow and both RhoA and Rac1 at cell-cell junctions in epithelial cells. *Mol. Biol. Cell* **26**, 2439-2455.

**Bryant, D. M., Datta, A., Rodríguez-Fraticelli, A. E., Peränen, J., Martín-Belmonte, F. and Mostov, K. E.** (2010). A molecular network for de novo generation of the apical surface and lumen. *Nat. Cell Biol.* **12**, 1035-1045.

**Burke, T. A., Christensen, J. R., Barone, E., Suarez, C., Sirotkin, V. and Kovar, D. R.** (2014). Homeostatic actin cytoskeleton networks are regulated by assembly factor competition for monomers. *Curr. Biol.* **24**, 579-585.

**Chailley, B., Nicolas, G. and Lainé, M.-C.** (1989). Organization of actin microfilaments in the apical border of oviduct ciliated cells. *Biol. Cell* **67**, 81-90.

**Chung, M.-I., Kwon, T., Tu, F., Brooks, E. R., Gupta, R., Meyer, M., Baker, J. C., Marcotte, E. M. and Wallingford, J. B.** (2014). Coordinated genomic control of ciliogenesis and cell movement by RFX2. *Elife* **3**, e01439.

**Datta, A., Bryant, D. M. and Mostov, K. E.** (2011). Molecular regulation of lumen morphogenesis. *Curr. Biol.* **21**, R126-R136.

**Drysdale, T. T. and Elinson, R. P.** (1992). Cell migration and induction in the development of the surface ectodermal pattern of the Xenopus laevis tadpole. *Dev. Growth Differ.* **34**, 51-59.

**Fritzsche, M., Lewalle, A., Duke, T., Kruse, K. and Charras, G.** (2013). Analysis of turnover dynamics of the submembranous actin cortex. *Mol. Biol. Cell.* **24**, 757-767.

**Fritzsche, M., Erlenkamper, C., Moeendarbary, E., Charras, G. and Kruse, K.** (2016). Actin kinetics shapes cortical network structure and mechanics. *Sci. Adv.* **2**, e1501337.

**Ganguly, A., Tang, Y., Wang, L., Ladt, K., Loi, J., Dargent, B., Leterrier, C. and Roy, S.** (2015). A dynamic formin-dependent deep F-actin network in axons. *J. Cell Biol.* **210**, 401-417.

**Goode, B. L. and Eck, M. J.** (2007). Mechanism and function of formins in the control of actin assembly. *Annu. Rev. Biochem.* **76**, 593-627.

**Grikscheit, K. and Grosse, R.** (2016). Formins at the Junction. *Trends Biochem. Sci.* **41**, 148-159.
**Grikscheit, K., Frank, T., Wang, Y. and Grosse, R.** (2015). Junctional actin assembly is mediated by Formin-like 2 downstream of Rac1. *J. Cell Biol.* **209**, 367-376.
**Hall, A.** (2012). Rho family GTPases. *Biochem. Soc. Trans.* **40**, 1378-1382.
**Higashi, T., Arnold, T. R., Stephenson, R. E., Dinshaw, K. M. and Miller, A. L.** (2016). Maintenance of the epithelial barrier and remodeling of cell-cell junctions during cytokinesis. *Curr. Biol.* **26**, 1829-1842.
**Kim, K., Lake, B. B., Haremaki, T., Weinstein, D. C. and Sokol, S. Y.** (2012). Rab11 regulates planar polarity and migratory behavior of multiciliated cells in Xenopus embryonic epidermis. *Dev. Dyn.* **241**, 1385-1395.
**Lai, F. P. L., Szczodrak, M., Block, J., Faix, J., Breitsprecher, D., Mannherz, H. G., Stradal, T. E. B., Dunn, G. A., Small, J. V. and Rottner, K.** (2008). Arp2/3 complex interactions and actin network turnover in lamellipodia. *EMBO J.* **27**, 982-992.
**Lomakin, A. J., Lee, K.-C., Han, S. J., Bui, D. A., Davidson, M., Mogilner, A. and Danuser, G.** (2015). Competition for actin between two distinct F-actin networks defines a bistable switch for cell polarization. *Nat. Cell Biol.* **17**, 1435-1445.
**Macara, I. G., Guyer, R., Richardson, G., Huo, Y. and Ahmed, S. M.** (2014). Epithelial homeostasis. *Curr. Biol.* **24**, R815-R825.
**Madrid, R., Aranda, J. F., Rodriguez-Fraticelli, A. E., Ventimiglia, L., Andrés-Delgado, L., Shehata, M., Fanayan, S., Shahheydari, H., Gomez, S., Jiménez, A. et al.** (2010). The formin INF2 regulates basolateral-to-apical transcytosis and lumen formation in association with Cdc42 and MAL2. *Dev. Cell* **18**, 814-827.
**Medioni, C., Astier, M., Zmojdzian, M., Jagla, K. and Sémériva, M.** (2008). Genetic control of cell morphogenesis during Drosophila melanogaster cardiac tube formation. *J. Cell Biol.* **182**, 249-261.
**Pan, J., You, Y., Huang, T. and Brody, S. L.** (2007). RhoA-mediated apical actin enrichment is required for ciliogenesis and promoted by Foxj1. *J. Cell Sci.* **120**, 1868-1876.
**Park, T. J., Haigo, S. L. and Wallingford, J. B.** (2006). Ciliogenesis defects in embryos lacking inturned or fuzzy function are associated with failure of planar cell polarity and Hedgehog signaling. *Nat. Genet.* **38**, 303-311.
**Park, T. J., Mitchell, B. J., Abitua, P. B., Kintner, C. and Wallingford, J. B.** (2008). Dishevelled controls apical docking and planar polarization of basal bodies in ciliated epithelial cells. *Nat. Genet.* **40**, 871-879.
**Pellettieri, J. and Sanchez Alvarado, A. A.** (2007). Cell turnover and adult tissue homeostasis: from humans to planarians. *Annu. Rev. Genet.* **41**, 83-105.
**Phng, L.-K., Gebala, V., Bentley, K., Philippides, A., Wacker, A., Mathivet, T., Sauteur, L., Stanchi, F., Belting, H.-G., Affolter, M. et al.** (2015). Formin-mediated actin polymerization at endothelial junctions is required for vessel lumen formation and stabilization. *Dev. Cell* **32**, 123-132.
**Reyes, C. C., Jin, M., Breznau, E. B., Espino, R., Delgado-Gonzalo, R., Goryachev, A. B. and Miller, A. L.** (2014). Anillin regulates cell-cell junction integrity by organizing junctional accumulation of Rho-GTP and actomyosin. *Curr. Biol.* **24**, 1263-1270.
**Rock, J. R., Onaitis, M. W., Rawlins, E. L., Lu, Y., Clark, C. P., Xue, Y., Randell, S. H. and Hogan, B. L. M.** (2009). Basal cells as stem cells of the mouse trachea and human airway epithelium. *Proc. Natl. Acad. Sci. USA* **106**, 12771-12775.
**Rock, J. R., Randell, S. H. and Hogan, B. L. M.** (2010). Airway basal stem cells: a perspective on their roles in epithelial homeostasis and remodeling. *Dis Model Mech.* **3**, 545-556.
**Rodriguez-Boulan, E. and Macara, I. G.** (2014). Organization and execution of the epithelial polarity programme. *Nat. Rev. Mol. Cell Biol.* **15**, 225-242.
**Rotty, J. D., Wu, C., Haynes, E. M., Suarez, C., Winkelman, J. D., Johnson, H. E., Haugh, J. M., Kovar, D. R. and Bear, J. E.** (2015). Profilin-1 serves as a gatekeeper for actin assembly by Arp2/3-dependent and -independent pathways. *Dev. Cell* **32**, 54-67.
**Sahasrabudhe, A., Ghate, K., Mutalik, S., Jacob, A. and Ghose, A.** (2016). Formin 2 regulates the stabilization of filopodial tip adhesions in growth cones and affects neuronal outgrowth and pathfinding in vivo. *Development* **143**, 449-460.
**Santiago-Martinez, E., Soplop, N. H., Patel, R. and Kramer, S. G.** (2008). Repulsion by Slit and Roundabout prevents Shotgun/E-cadherin-mediated cell adhesion during Drosophila heart tube lumen formation. *J. Cell Biol.* **182**, 241-248.
**Sedzinski, J., Hannezo, E., Tu, F., Biro, M. and Wallingford, J. B.** (2016). Emergence of an apical epithelial cell surface in vivo. *Dev. Cell* **36**, 24-35.
**Sirour, C., Hidalgo, M., Bello, V., Buisson, N., Darribere, T. and Moreau, N.** (2011). Dystroglycan is involved in skin morphogenesis downstream of the Notch signaling pathway. *Mol. Biol. Cell.* **22**, 2957-2969.
**Stubbs, J. L., Davidson, L., Keller, R. and Kintner, C.** (2006). Radial intercalation of ciliated cells during Xenopus skin development. *Development* **133**, 2507-2515.
**Suarez, C., Carroll, R. T., Burke, T. A., Christensen, J. R., Bestul, A. J., Sees, J. A., James, M. L., Sirotkin, V. and Kovar, D. R.** (2015). Profilin regulates F-actin network homeostasis by favoring formin over Arp2/3 complex. *Dev. Cell* **32**, 43-53.
**Taniguchi, K., Shao, Y., Townshend, R. F., Tsai, Y.-H., DeLong, C. J., Lopez, S. A., Gayen, S., Freddo, A. M., Chue, D. J., Thomas, D. J. et al.** (2015). Lumen formation is an intrinsic property of isolated human pluripotent stem cells. *Stem Cell Reports* **5**, 954-962.
**Turk, E., Wills, A. A., Kwon, T., Sedzinski, J., Wallingford, J. B. and Stearns, T.** (2015). Zeta-tubulin is a member of a conserved tubulin module and is a component of the centriolar basal foot in multiciliated cells. *Curr. Biol.* **25**, 2177-2183.
**Watanabe, N.** (2010). Inside view of cell locomotion through single-molecule: fast F-/G-actin cycle and G-actin regulation of polymer restoration. *Proc. Jpn. Acad. Ser. B Phys. Biol. Sci.* **86**, 62-83.
**Watson, J. K., Rulands, S., Wilkinson, A. C., Wuidart, A., Ousset, M., Van Keymeulen, A., Gottgens, B., Blanpain, C., Simons, B. D. and Rawlins, E. L.** (2015). Clonal dynamics reveal two distinct populations of basal cells in slow-turnover airway epithelium. *Cell Rep.* **12**, 90-101.
**Werner, M. E. and Mitchell, B. J.** (2011). Understanding ciliated epithelia: the power of Xenopus. *Genesis* **50**, 176-185.
**Werner, M. E., Hwang, P., Huisman, F., Taborek, P., Yu, C. C. and Mitchell, B. J.** (2011). Actin and microtubules drive differential aspects of planar cell polarity in multiciliated cells. *J. Cell Biol.* **195**, 19-26.
**Werner, M. E., Mitchell, J. W., Putzbach, W., Bacon, E., Kim, S. K. and Mitchell, B. J.** (2014). Radial intercalation is regulated by the Par complex and the microtubule-stabilizing protein CLAMP/Spef1. *J. Cell Biol.* **206**, 367-376.
**Yang, C., Czech, L., Gerboth, S., Kojima, S.-i., Scita, G. and Svitkina, T.** (2007). Novel roles of formin mDia2 in lamellipodia and filopodia formation in motile cells. *PLoS Biol.* **5**, e317.

# SUPPLEMENTARY FIGURES

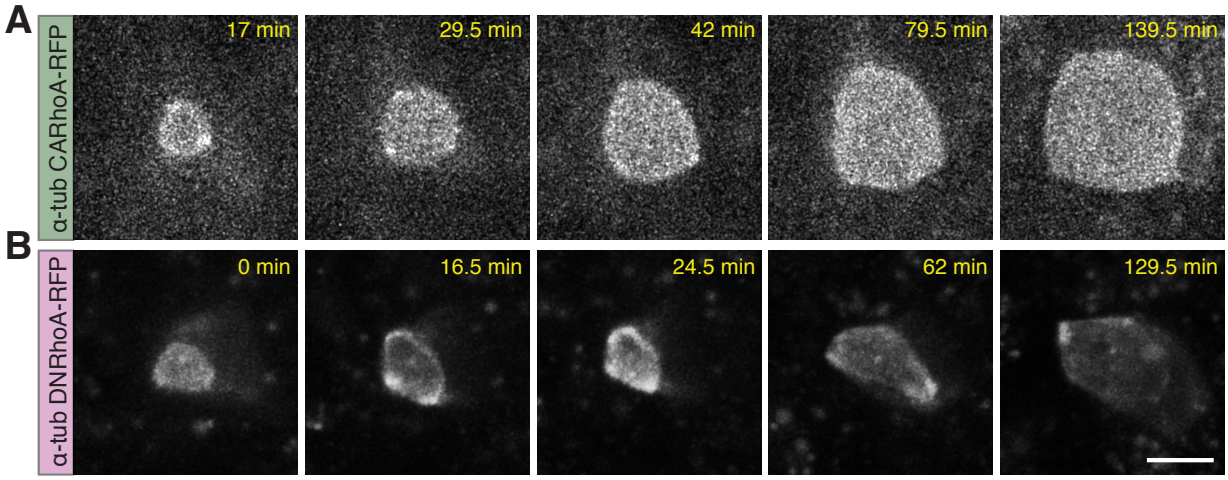


**Figure S1. RhoA regulates apical emergence dynamics.** (A) Image sequence of an apically emerging MCC upon expression of CA-RhoA-RFP specifically in MCC using a MCC-specific $\alpha$-tubulin promoter. (B) Image sequence of an apically emerging MCC upon expression of DN-RhoA-RFP specifically in MCC using a MCC-specific $\alpha$-tubulin promoter. Scale bar, 10 µm.

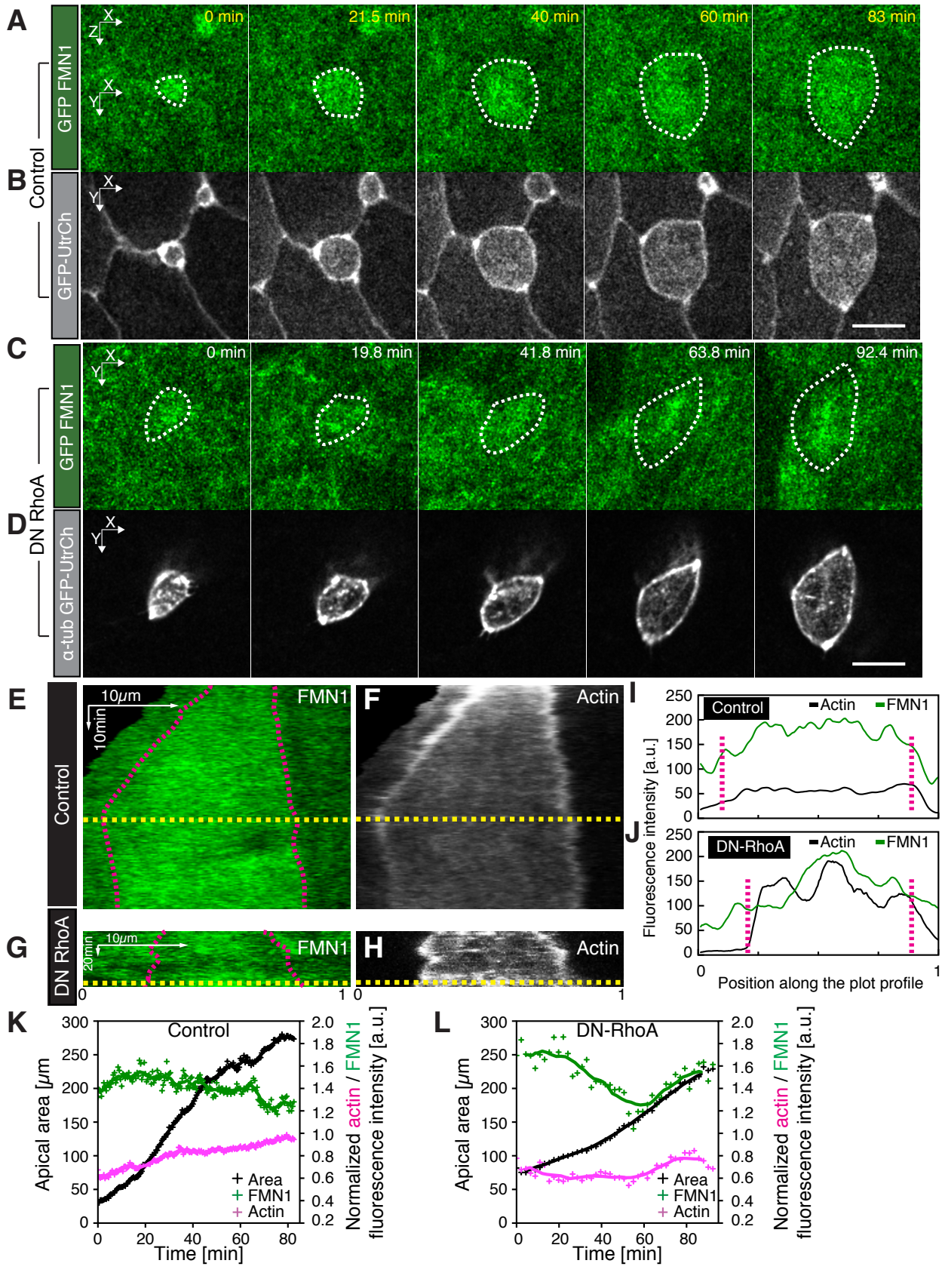
A
B
Control
GFP FMN1
GFP-UtrCh
0 min
21.5 min
40 min
60 min
83 min
C
D
DN RhoA
GFP FMN1
α-tub GFP-UtrCh
0 min
19.8 min
41.8 min
63.8 min
92.4 min
E
Control
10μm
10min
FMN1
F
Actin
G
DN RhoA
10μm
20min
FMN1
H
Actin
I
Control
Actin
FMN1
J
DN-RhoA
Actin
FMN1
Fluorescence intensity [a.u.]
Position along the plot profile
K
Control
Apical area [μm
Normalized actin / FMN1 fluorescence intensity [a.u.]
Area
FMN1
Actin
Time [min]
L
DN-RhoA
Apical area [μm
Normalized actin / FMN1 fluorescence intensity [a.u.]
Area
FMN1
Actin
Time [min]

**Figure S2. Expression of DN-RhoA impairs the localization and dynamics of formin 1.** (A) Image sequence of fluorescently labelled Fmn1 (green) during apical emergence in a control cell. (B) Image sequence of an apically emerging control cell visualized with an actin marker, UtrCH (grey). (C) Image sequence of fluorescently labelled Fmn1 (green) during apical emergence upon expression of DN-RhoA. (D) Image sequence of an apically emerging cell visualized with actin marker, UtrCH (grey) upon expression of DN-RhoA. (E) Kymograph of FMN1 signal during apical expansion of a control cell. (F) Kymograph of actin signal (visualized by UtrCH) in a control cell. (G) Kymograph of FMN1 signal upon expression of DN-RhoA. (H) Kymograph of actin signal (visualized by UtrCH) upon expression of DN-RhoA. (I) Formin 1 and actin (visualized by UtrCH) fluorescence intensity profile along the apical domain diameter (yellow dotted line, starts at 0 and ends at 1) in controls and upon expression of DN-RhoA (J). (K) Dynamics of Fmn1 and actin in controls and upon expression of DN-RhoA (L). Scale bar, 10 µm.

**Table S1. Frequency of apical domain collapses and partial collapses in various experimental conditions.** Apical domain partially collapses - the apical surface undergoes non-periodic damped oscillations, it expands and shrinks but does not fully collapse.

| Conditions | % of collapsing / partially collapsing cells | *n = |
|---|---|---|
| Controls | 0 / 3.3 | 30 |
| α-tubulin CARhoA | 0 / 3.3 | 23 |
| α-tubulin DNRhoA | 7 / 34.5 | 29 |
| Formin 1 KD | 30.6 / 20.4 | 49 |

* From n > 5 embryos

# SUPPLEMENTARY MOVIE

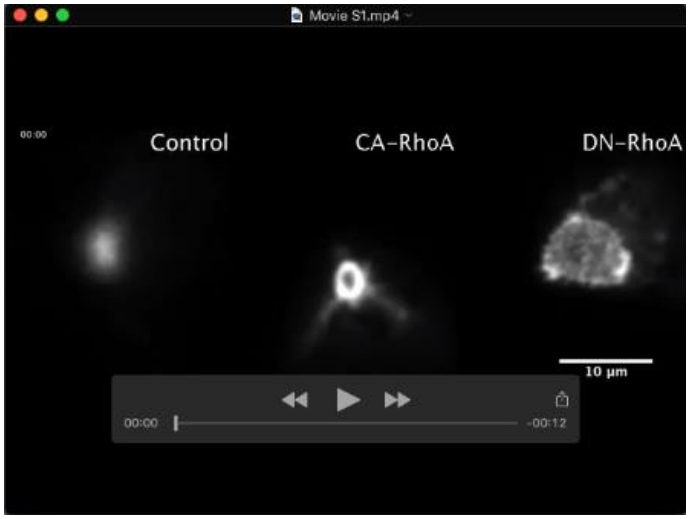


**Movie 1. Apical emergence of nascent multiciliated cells (MCCs) within *Xenopus laevis* epithelium.** Time-lapse movie of an apically expanding MCC (visualized by $\alpha$-tubulin UtrCH-GFP, grey) in controls, upon expression of CA-RhoA, and DN-RhoA. Scale bar, 10 µm.